Spatial Structure Characterization of the Soil Surrounding Buried Water Transmission Mains by Using a Sensor-Enabled Geotextile

Humberto Yáñez-Godoy, Sidi Mohammed Elachachi

Spatial structure characterization of the soil surrounding buried water-transmission mains by using a sensor-enabled geotextile

Humberto Yáñez-Godoy[1] and Sidi Mohammed Elachachi[2]

[1] Associate Professor, Univ. of Bordeaux, Institute of Mechanical Engineering (I2M), UMR 5295, Bât. A11, 351 Cours de la Libération, 33405 Talence Cedex, France (corresponding author). ORCID: https://orcid.org /0000-0001-9918-3457. Email: humberto.yanez-godoy@u-bordeaux.fr

[2] Professor, Univ. of Bordeaux, Institute of Mechanical Engineering (I2M), UMR 5295, Bât. A11, 351 Cours de la Libération, 33405 Talence Cedex, France. Email: sidi-mohammed.elachachi@u-bordeaux.fr

Abstract: Close examination of the parameters that characterize the spatial variability of the soil is necessary to understand how this vari- ability can be used to study the structural behavior of buried large-diameter water transmission mains. In this research, a sensor-enabled geotextile was laid in a trench along a renewed water transmission pipeline segment to measure the ground strain during its installation and the first months of pipeline operation. A methodological approach was developed to identify, from experimental semivariograms built from ground strain measurement profiles, the scale of fluctuation that characterizes the horizontal spatial structure of the soil. Using both an experimental onsite test and a numerical model of the pipeline, the spatial variability was assumed to correspond to the soil modulus param- eter in the model. The numerical results were well matched with the experimental test measurements. Both parameters, the scale of fluctuation and the soil modulus, were identified as important factors for understanding the spatial behavior of the soil–pipe system.

Journal of Pipeline Systems Engineering and Practice, Volume 14, Issue 3, https://doi.org/10.1061/JPSEA2.PSENG-1409

Practical Applications: Soil heterogeneity affects the structural response of a buried pipe with respect to force redistribution and structural displacement, and its influence appears mainly in the longitudinal direction. This heterogeneity results in the spatial variability of soil proper- ties. Furthermore, the geomechanical behavior of buried pipes is subject to random uncertainties. In the framework of this study, the uncertain variables are treated by the theory of probabilities. Such an approach can be integrated into the context of asset management of a network of water transmission pipes. Thus, wishing optimized management of a network, the project manager needs a tool allowing him to evaluate the geomechanical performance of the pipes and to see if it is necessary to proceed to a follow-up in terms of inspection, maintenance, or renewal. This study showed that both soil modulus and the horizontal correlation length parameter of soil properties could characterize the spatial variability of a pipe site. By integrating these parameters into a numerical tool, a manager can incorporate spatial variability in a simple way while maintaining full control over their variability.

INTRODUCTION

Renewal of aged drinking water pipes is necessary to ensure sustained access to drinking water services with both high quality and high performance. The gradual decline in the performance of aged pipes is not always clear in practice, especially for large-diameter water transmission pipelines, called feeders (i.e., pipes that are used as major water transmission mains and have diameters between 0.3 m and 4 m), even if the available data are valuable for predicting feeder failures (Romer et al. 2007; Higgins et al. 2012; Rajeev and Kodikara 2014). To predict the structural degradation of a feeder by deterministic or probabilistic approaches, two types of models can be used to assess the failure probability (Liu et al. 2012): physical/mechanical models and statistical/empirical models. Physical models attempt to recreate the loading and environmental conditions that are the most similar to the actual conditions to which buried pipes are often subjected (Rajani and Kleiner 2001). Although these models are robust, reliable, and efficient, they are limited by both existing expertise and the availability of data (loading forces and environmental properties). Furthermore, data collection is quite expensive and labor-intensive, but it can be justified due to the cost of a potential defect or feeder dysfunction. Statistical models can be useful for assessing the integrity of distribution water mains when the failure frequency is much higher than that of feeders, but the cost of defaults is lower than that of feeders and does not justify data collection campaigns (Kleiner and Rajani 2001). Owing to the limited number of failures and the unavailability of extensive databases of feeder failures, it is appropriate to focus on physical models to assess and predict structural degradation and to integrate the spatial variability of material properties. Indeed, physical models offer the ability to model pipe degradation for different material components, such as steel and concrete, and can easily be adapted to integrate spatial variability using probabilistic approaches (Aslkhalili et al. 2021; Wang et al. 2021; Sahraoui et al. 2020; Oswell et al. 2019). To ensure the safe design of a new pipe or to evaluate the residual life of an existing buried pipe, a reliable assessment of the soil stresses on the pipe due to soil–pipe displacements is necessary (Zheng et al. 2021). However, one must recall that the behavior of a pipeline depends on the stiffness and structural behavior of each pipe segment (i.e., materials and joints) and the nature of the soil displacements (Becerril García et al. 2020; Xu and Shen 2020). Rigid and flexible pipes are vulnerable to stresses generated by soil displacements. Soil compaction is often underestimated or neglected during pipe design, and spatial variability is not considered.

The parameters necessary to model the spatial variability must be identified before studying the structural behavior of a buried pipe to help elucidate the complexity of the soil–pipe system and its interactions (McGrath et al. 1990; Elachachi et al. 2012), where the soil is a principal component of the system and can absorb a large proportion of the load. The behavior modeling of the soil–pipe system interactions is a three-dimensional complex problem that requires sophisticated numerical models that are expected to utilize well-featured soil models (e.g., the linear elastic–perfectly plastic model, Cam-Clay modified model, nonlinear elastic model, and linear elastic–hardening plasticity model). Soil is a multiphase material whose behavior is not as predictable as that of other materials such as steel and concrete, and its properties may vary significantly from one site to another. Furthermore, soil is a heterogeneous material and is the predominant source of both

uncertainty and variability in an area in which pipes are laid. Spatial variability may also involve regionalized data (Breysse et al. 2007), meaning that the measured soil properties (e.g., soil modulus, permeability coefficient, porosity, internal friction angle, and water content) at two neighboring points are statistically more similar than those at two distant points, in both the vertical and horizontal directions. The soil properties can then be considered spatially structured. This assumption enables the use of approaches such as an autocorrelation function (from random field theory) or a semivariogram function (from geostatistics) that can be employed to identify the distance at which the soil properties become independent or uncorrelated (Elachachi et al. 2012; Onyejekwe et al. 2016). This distance, known as the scale of fluctuation (Vanmarcke 1977), defines the distance over which there are significant correlations between material properties.

The spatial variability of geotechnical parameters is generally determined by the scale of fluctuation and can be obtained by analyzing the spatial variability of the measurement profiles (Jaksa et al. 1999; Onyejekwe et al. 2016; Bouayad 2017; Ching et al. 2018). It is preferred to use a semivariogram function instead of an autocorrelation function to determine the scale of fluctuation because the former is an unbiased estimator and does not depend on the mean of the data set. In addition, a semivariogram function requires a less restrictive statistical assumption regarding stationarity than an autocovariance function (Uzielli et al. 2007; Chilès and Delfiner 2012). This semivariogram [Fig. 5(b)] gives the mean of the halved squared increment as a function of distance. This curve is characterized by the nugget effect parameter (which is the height of the jump of the semivariogram at the discontinuity at the origin), sill parameter (which is the limit to which the variogram tends at infinite lag distances), and the range influence or correlation length (which is the distance at which samples become independent of one another). Theoretical semivariogram models are available to fit empirical or experimental semivariogram samples (Onyejekwe et al. 2016). Random field theory combined with the semivariogram function can also be useful to simulate several semivariograms by utilizing Monte Carlo methods to obtain the best fit to the experimental semivariogram sample. The parameters characterizing the experimental semivariogram, such as the scale of fluctuation, are then searched using the least-squares method.

A replaced feeder segment in Paris, France, was the subject of study in this article. One of the principal requirements regarding the instrumented area in which the feeder is laid was to identify the parameters that characterize the spatial variability of the soil. To improve understanding of these factors, the objectives of the research presented in this paper were (1) to instrument the soil–pipe system during the construction stage with a sensor-enabled geotextile; (2) to measure the ground strains along the pipeline at different dates; and (3) to identify the parameters that characterize the spatial structure of the soil. The remainder of this article is organized as follows. The first section describes the study area where the renewed water transmission pipeline segment is located and gives an idealization of the modeling. The second section presents the instrumentation technology used to study the soil–pipe system. The third section presents ground strain measurements. The fourth section discusses the statistical tools for the analysis of measures and presents a numerical mechanical model used in this study. The fifth section describes the methodological approach used to identify the parameters characterizing the horizontal spatial structure of soil and

explains to which soil parameter corresponds to the variability using both an experimental onsite test and a numerical model of the instrumented pipeline. Finally, the conclusions are presented in the sixth section.

IDEALIZATION OF THE MODELING

The replaced water-transmission pipeline segment studied in this paper forms part of the drinking water network owned by the Syndicat des Eaux d'Île-de-France. It is a reinforced concrete steel cylinder pipe (i.e. a steel cylinder is embedded in a concrete core (Yáñez-Godoy et al. 2017a; Darwich 2019), 90 m long, has an inner diameter of 800 mm, with a thickness of 0.072 m, and is composed of pipes with a mean length of approximately 6 m. These pipes are also known as bonna pipes and are designed and manufactured according to the recommendations of French standards, NF EN 1295-1 (Afnor 2019), NF EN 639 (Afnor 1995a) and NF EN 641 (Afnor 1995b). The pipeline is a concrete pressurized pipe located in Saint-Denis, a commune in the northern suburbs of Paris, France. The main axial plane of the pipeline is adjacent to an important traffic lane. The pipe and surrounding ground in the trench were considered as the soil–pipe system to be instrumented. The cross-section of the pipeline is presented in Figure 1a, along with the locations of the two sensor-enabled geotextiles used in this project (above and below the pipeline). The mean depth at which the pipe is buried is about 2.5 m. The final location of the pipeline specified that the "trench type" section meets the requirements of a trench under a main road, according to the French standard NF P38-331 (Afnor 2020). The compaction tests, during the initial phase of replacement, showed that, with respect to the compaction objectives and the classification of the materials used, it was necessary to reinforce the characteristics of the backfill with cement-treated gravel over its entire thickness. The main backfill (Fig. 1a**)** is composed of two layers of cement-treated base: the cement content for stabilization is 3% in the first layer and 5% in the second layer. The pipe is embedded in a sand-filled trench (embedment layer).

In this study it was assumed that the soil–pipe system in Figure 1a is represented by the schematic views of Figure 1b (pipeline cross-section) and Figure 1c (pipeline length). In these figures, each layer above and below the pipeline and the pipe itself occupy a domain Ω_n, where *n* is a component of the soil–pipe system. Each domain Ω_n, was considered as a homogeneous element equivalent to the soil or to the pipe. The spatial variability of soil is necessary to understand how this variability can be used to study the structural behavior of the buried pipeline. To identify this variability a sensor-enabled geotextile was then placed in each soil domain and allowed to measure the deformations of the ground surrounding the pipeline along and across the trench where the pipe was laid. Once the signal has been obtained, statistical tools as a semivariogram function could be used to identify a possible correlation between the different points of the signal. This analysis leads to the identification of a signal correlation length value where random fields are needed to model the spatial variability of the soil. Indeed, a random field assumed to be spatially correlated could be associated with an autocorrelation function in which a correlation length value is considered as generating a random process.

Many soil properties such as permeability coefficient, porosity, internal friction angle, moisture content could show spatial variability. In this study, soil modulus (a geomechanical property) is indirectly dependent on soil density and soil moisture (physical properties). Therefore, its spatial variability is correlated with their respective spatial variability. The soil modulus was then assumed to characterize the spatial randomness of the soil. The soil-pipe system shown in Figure 1c could even be modelled by a more simplified model, as shown in Figure 1d, which is less computationally intensive for structural reliability analysis. This model is based on beam theory where the individual pipe segments are modelled by beam elements and the soil-structure interaction by springs with a stiffness or subgrade reaction coefficient that depends on the soil modulus. As the soil is a nonlinear and non-homogeneous material, the subgrade reaction coefficient can be approached by semi-empirical (Elachachi et al. 2004) or analytical methods (Froio and Rizzi 2017) or consider nonlinear Winkler spring model of the soil, where an elastic-perfectly plastic force-deformation relationship is assumed (Joshi et al. 2011). The two-dimensional model shown in Figure 1c which considers the two soil layers above and below the pipeline was chosen for the numerical analysis in this paper. This model has limitations in assessing the overall structural integrity of the pipe. Indeed, only the stresses and displacements are evaluated in the longitudinal direction and not in the cross-section of the pipe. The modeling of the pipe joints (steel joints, according to (Afnor 1995b)) is only performed at the interface between the pipe and the joint. These details are presented in the section “Two-dimensional finite element model”. The main purpose of this two-dimensional model is not to evaluate the effect of spatial variability of soil on the overall structural integrity of the pipe, but to verify the ground strain measurements obtained on the site, during a static load test of a truck parked at different positions on the main axis of the pipe. Indeed, the identified soil factors (presented in section “Identification of soil spatial variability from measurements”) enable spatial variability characterization along the length and width of the trench in which the pipeline is laid.

MONITORING SOLUTION TO STUDY SPATIAL VARIABILITY OF SOIL

This section presents both the instrumentation technology used to study the soil–pipe system and its implementation in the study area. A Brillouin-distributed optical fiber sensor was utilized for measurement (Galindez-Jamioy and López-Higuera 2012; Iten et al. 2015). The Brillouin scattering of light was employed to measure the strain in the optical fibers. Ground strains can originate from ground settlement or temperature variations. The sensor-enabled geotextile used in this project to measure the ground strain contained two strips of geotextiles. Four optical fiber cables were embedded in each trip. The high friction properties of the soil-textile interface and the strong bond between the optical cable and the geotextile allow the transfer and detection of very small soil strains. Even if the advantage of the geotextile is to contribute to the drainage and the reinforcement of the ground with its hydraulic (drainage in the plane) and mechanical functions (friction with the ground), soil behavior is assumed to be unchanged.

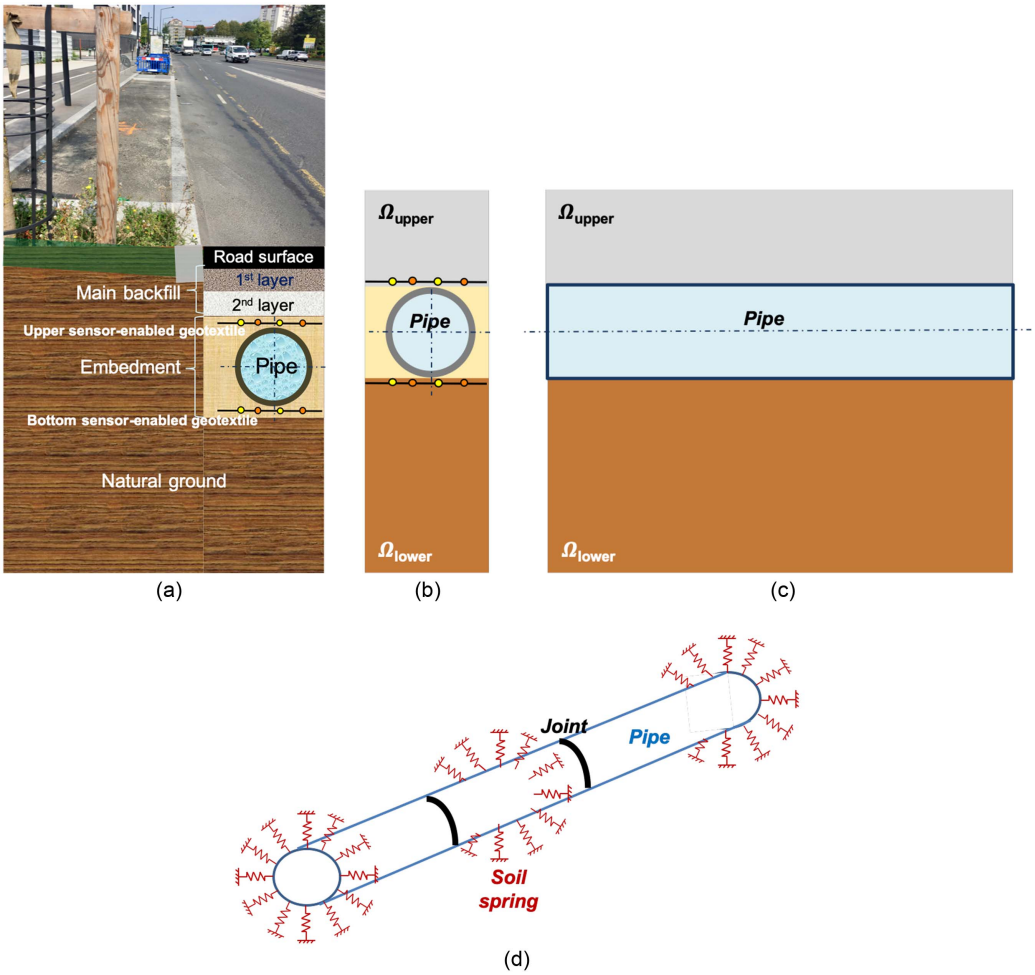

Fig. 1. *Soil–pipe system: (a) pipe and surrounding ground in the trench (image by Humberto Yáñez-Godoy); (b) cross section; (c) longitudinal section; and (d) pipe and soil-interaction model.*

The spatial resolution of the optical fiber cable measurements was 20 cm. The optical fiber cable loops used to measure the ground strain were yellow and orange (Fig. 2a). The yellow loop was the main measuring loop, and the orange one was a redundant measuring loop. The ground strain in the axial plane of the pipeline was measured by the sensor-enabled geotextile, which was placed below and above the pipeline (Fig. 2b and Fig. 2d) between two sand layers 10 cm thick. The bottom layer was compacted to prevent any deformation of the optical fiber during the implementation of the geotextile on the site. The characteristics of the backfill having been reinforced with cement-treated gravel over its entire thickness, the fact of having compacted the layer under the geotextile provided a good support for its placement and does not significantly modify the stiffness of the surrounding soil.

The sensor-enabled geotextile measured the ground strain through the friction exerted between the geotextile and soil, as well as the Brillouin light backscattered along the optical fiber cable. Indeed, although most of the light pulse injected into the optical fiber core was transmitted from one end to the other, a small amount of friction was backscattered toward the source owing to imperfections in the density of the fiber. The Brillouin scattering peaks were analyzed to measure the strain changes along the fiber. The Brillouin frequency shift, υ_i, between two measurements at a reference time, T_0, and a given time, T_i, can be obtained as follows at any point along the optical fiber cable (Eq. 1):

$$\upsilon_i(T_i, \varepsilon_i) = C_\varepsilon \Delta\varepsilon_i + C_T \Delta T_i + \upsilon_0(T_0, \varepsilon_0) \quad (1)$$

where υ_i depends on both the applied strain variation, $\Delta\varepsilon_i$, and the temperature variation, ΔT_i; υ_0 is the Brillouin frequency at T_0; and $C_\varepsilon = 0.02$ MHz/με and $C_T = 1$ MHz/°C are the constant strain and temperature coefficients, respectively. The temperature can also be obtained by the sensor (black and blue optical fiber cables shown in Fig. 2a); however, this parameter was not measured because the depth of the geotextile implanted in the soil ensures a steady temperature within ±5 °C. The strain variation at T_i can be expressed as follows (Eq. 2):

$$\Delta\varepsilon_i = \frac{\Delta\upsilon_i}{C_\varepsilon} \quad (2)$$

where $\Delta\upsilon_i = \upsilon_i(T_i, \varepsilon_i) - \upsilon_0(T_0, \varepsilon_0)$ is the Brillouin frequency variation at T_i.

Fig. 2. *Sensor-enabled geotextile and its location (FOND means below, DESSUS means above, ROUTE means roadside, and TROTTOIR means sidewalk side): (a) sensor-enabled geotextile; (b) sensor below the pipeline; (c) location of measuring-loop optical cables (below the pipeline); (d) sensor above the pipeline; and (e) location of measuring-loop optical cables (above the pipeline).*

GROUND STRAIN MEASUREMENTS

Three horizontal ground strain measurements were conducted in December 2016, June 2017, and August 2017. The sensor-enabled geotextile (Fig. 2a) consisted of two strips: the left strip (LS), placed on the sidewalk side, and the right strip (RS), placed on the roadside. To distinguish the optical fiber cable loops in each strip (yellow, Y, and orange, O) and the geotextile position to the axial plane of the pipe (above, A, and below, B) the following tetragram was used: ALSY (above left strip yellow), ARSY (above right strip yellow), ALSO (above left strip orange), ARSO (above right strip orange), not used in the project because the cable was unusable, BLSY (below left strip yellow), BRSY (below right strip yellow), BLSO (below left strip orange) and BRSO (below right strip orange). The location of the sensor-enabled geotextile below and above the pipeline was not constant and could vary by $\pm$10 cm relative to the axial plane of the pipeline (Fig. 2c and Fig. 2e). The measuring-loop optical cables were separated by approximately 27 cm, which enabled us to obtain measurements across the entire width of the ground above the pipeline.

The horizontal ground strain measurements obtained above and below the axial plane of the pipeline on three different dates are presented in Figure 3 and Figure 4. The measurements performed in December 2016 show very low strains in relation to the reference measurement conducted in October 2016, specifically $\pm$2000 µm/m, that is, $\pm$0.2%. Some local strains are very important at certain points, for example, at 12 m, 34 m, and 13 m for the ALSY, ARSY, and ALSO series (Fig. 3a, Fig. 3b and Fig. 3c) and at 48 m, between 35 and 70 m, at 65 m, and between 40 m and 65 m for the BLSY, BRSY, BLSO, and BRSO series (Fig. 4a, Fig. 4b, Fig. 4c and Fig. 4d), respectively. The measurements conducted in June 2017 exhibit a more significant increase than those obtained in December 2016, and the local strains are even more important for some profiles, for example, between 10 m and 30 m, 30 m and 40 m, and 0 m and 15 m for the ALSY, ARSY, and ALSO series, respectively. The local point strain values mentioned earlier for the BLSY, BRSY, BLSO, and BRSO series are even higher. The series of left strips (ALSY, ALSO, BLSY, BLSO), i.e., on the sidewalk side, do not seem to present a homogeneous orientation curve between them; in fact, some local strains are more disproportionate than the general trend line. It is possible that the loads were more concentrated on the sidewalk side during the work period. The strain variation between June 2017 and August 2017 is very low, which enables us to assume the stability of differential settlements above and along the pipeline (i.e., data stationarity). The profile acquired in June 2017 was retained for a more detailed analysis of the spatial structure of the soil.

STATISTICAL TOOLS AND FINITE ELEMENT MODEL FOR ANALYSIS OF MEASURES

Spatial variability approach: fast Fourier transform method to model soil spatial variability

A random field, $\varepsilon_x(x)$, representing the spatial ground strain measurements (above or below the pipeline) in the horizontal direction of the pipeline was generated using the fast Fourier transform (FFT) method (Yang 1972), which is one means of representing soil spatial

variability. The normal random field, $\varepsilon_x(x)$, passes through the beta inverse cumulative distribution function, F^{-1}, which was obtained as follows (Eq. 3):

$$\varepsilon_x(x) = F^{-1}\big(F(M(x)|\mu,\sigma)\big) \tag{3}$$

where $F(M(x)|\mu,\sigma)$ is the cumulative distribution function of a zero-mean, μ, normal random process, $M(x)$, with standard deviation, σ. The generated $M(x)$ process is associated with an autocorrelation function, $\rho(\tau)$, where τ is the distance between data points in the random field. Different common models of the autocorrelation function can be considered (Phoon 2014; Nie et al. 2015) as shown in Table 1, where δ_h is the correlation length associated with the model in the horizontal direction of the soil. δ_h can be obtained using a statistical tool known as a semivariogram, which is presented in the next section. δ_h is related to the scale of fluctuation, θ, based on the appropriate relationship for the chosen model. As an example, Figure 5a presents the case of a random field, $\varepsilon_x(x)$, with $\theta = 5$ m, considering the different models of the autocorrelation function; where SE: single exponential model, BN: binary noise model, CE: cosine exponential model, SOM: second-order Markov model and SqE: squared exponential model.

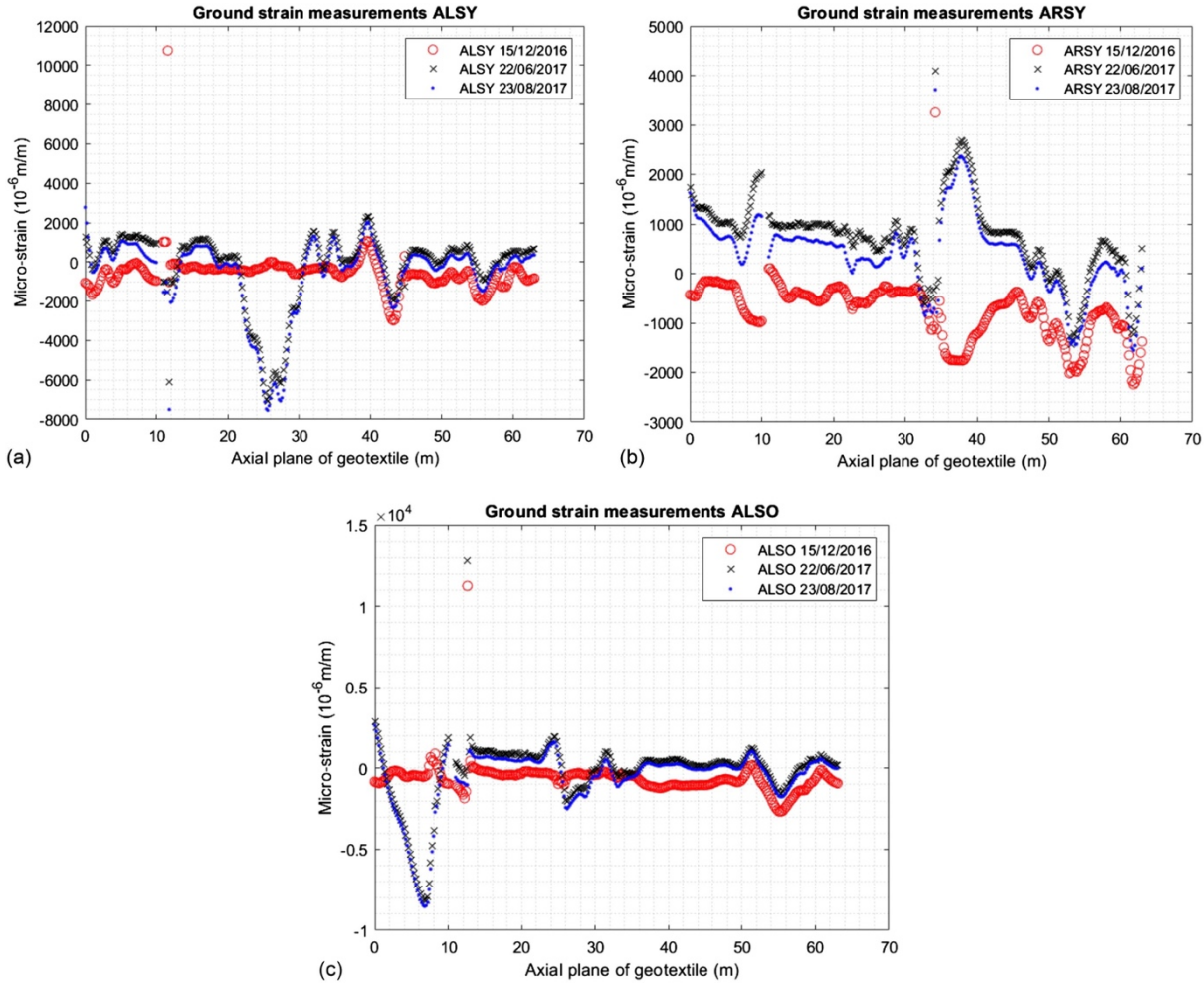

Fig. 3. *Ground strain measurements above the pipeline on three different dates: (a) above LS yellow, ALSY series; (b) above RS yellow, ARSY series; and (c) above LS orange, ALSO series.*

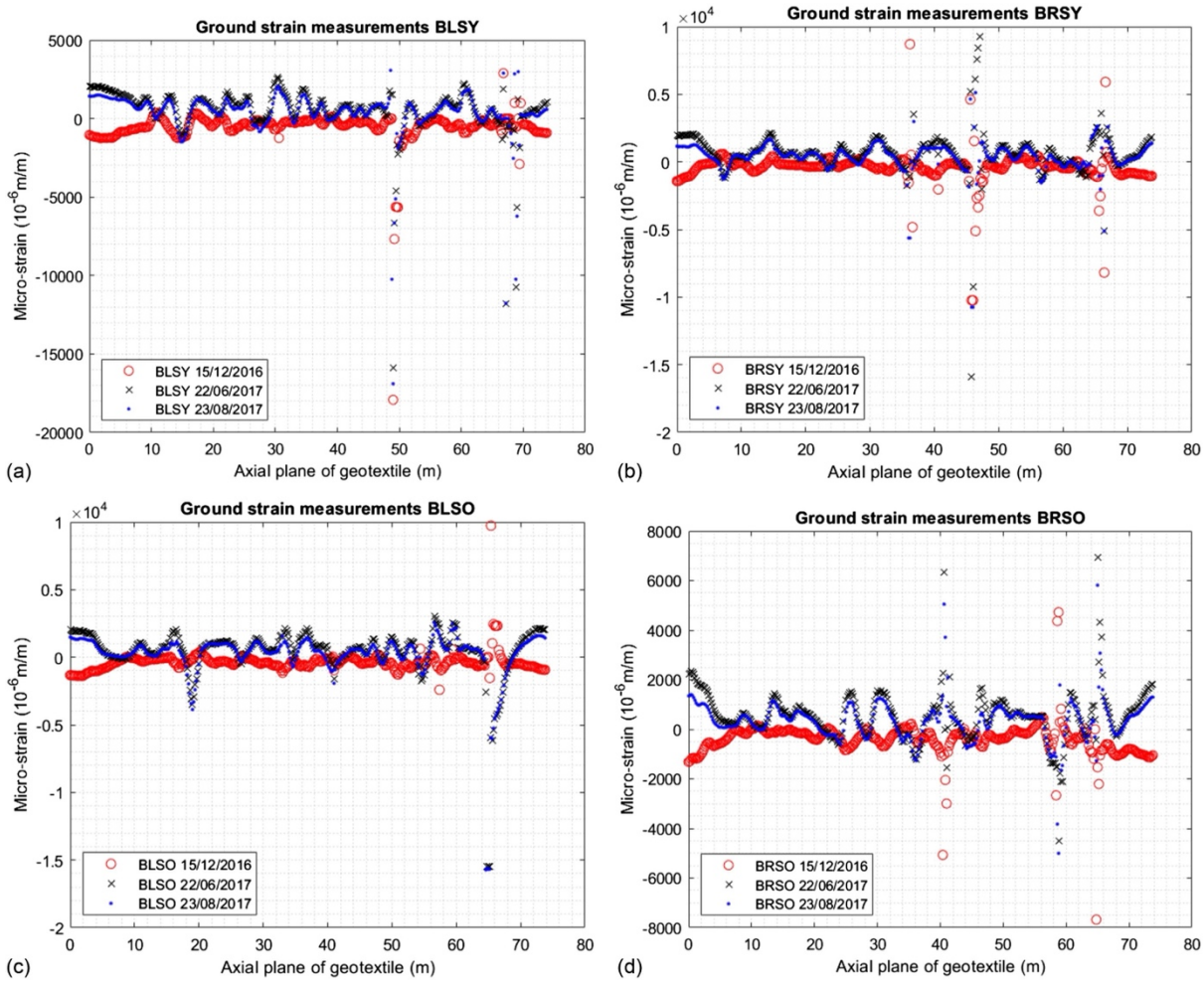

Fig. 4. *Ground strain measurements below the pipeline on three different dates: (a) below LS yellow, BLSY series; (b) below RS yellow, BRSY series; (c) below LS orange, BLSO series; and (d) below RS orange, BRSO series.*

Table 1. *Common autocorrelation function models.*

Model name	Autocorrelation function	Scale of fluctuation, θ
Single exponential	$\rho(\tau) = \exp\left(-\lvert\tau\rvert \cdot {\delta_h}^{-1}\right)$	$\theta = 2\delta_h$
Binary noise	$\rho(\tau) = \begin{cases} 1 - \lvert\tau\rvert \cdot {\delta_h}^{-1} & \text{if } \lvert\tau\rvert \le \delta_h \\ 0 & \text{if } \lvert\tau\rvert > \delta_h \end{cases}$	$\theta = \delta_h$
Cosine exponential	$\rho(\tau) = \exp\left(-\lvert\tau\rvert \cdot {\delta_h}^{-1}\right) \cdot \cos\left(\tau \cdot {\delta_h}^{-1}\right)$	$\theta = \delta_h$
Second-order Markov	$\rho(\tau) = \exp\left(-\lvert\tau\rvert \cdot {\delta_h}^{-1}\right) \cdot \left(1 + \lvert\tau\rvert \cdot {\delta_h}^{-1}\right)$	$\theta = 4\delta_h$
Squared exponential	$\rho(\tau) = \exp\left(-\left(\lvert\tau\rvert \cdot {\delta_h}^{-1}\right)^2\right)$	$\theta = \sqrt{\pi}\delta_h$

Statistical tool: empirical semivariogram

An empirical semivariogram is a statistical tool that characterizes the spatial structure of soil (Cressie 2015; Grynyshyna-Poliuga 2019). The empirical semivariogram is characterized by the function $\gamma(h)$, which describes the degree of spatial dependence of the spatial series. For a spatial series, the covariance between points is computed and enables analysis of how the acquired information deteriorates at one point when moving away from another. The semivariogram of variable Z for lag h between two adjacent points, (x) and $(x + h)$, is computed as follows (Eq. 4):

$$\gamma(h) = \frac{1}{2} \times E\left[\left(Z(x+h) - Z(x)\right)^2\right] \qquad (4)$$

where $E[(.)^2]$ is the expectation of the squared increment of the values between (*x*) and (*x + h*). In the empirical semivariogram model (Fig. 5b), the curve levels out after a certain distance known as the range or correlation length, δ. This characteristic means that sample locations that are separated by a distance smaller than the correlation length are spatially autocorrelated, whereas sample locations that are farther apart than the range can be considered spatially independent. The sill or semivariance value on the y-axis, *v*, is the value or limit that the empirical semivariogram attains an infinity distance.

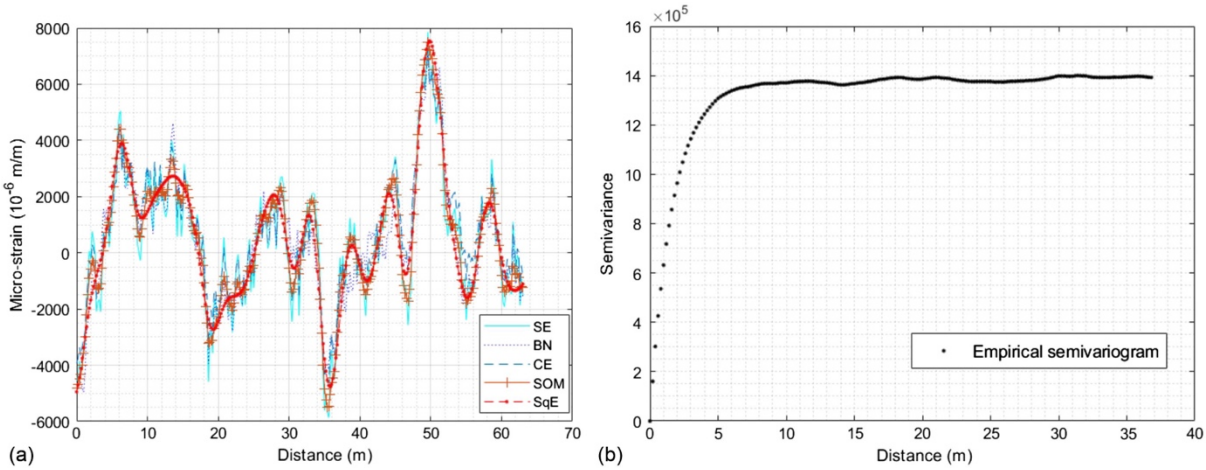

Fig. 5. *Examples of a random field of ground strain variations along a pipeline considering different autocorrelation function models and an empirical semivariogram: (a) random field for ϑ = 5 m; and (b) empirical semivariogram.*

Two-dimensional finite element model

The two-dimensional numerical mechanical model used in this study allowed to simulate a concrete pipeline buried in a soil. It represented approximately half the length of the pipeline in the study area. This model was coded within the finite element computer code CAST3M. As mentioned in section "Idealization of the modeling", the final location of the main axis of the pipe specified that the "trench type" section corresponds to the requirements of a trench under a heavy road. The characteristics of the backfill were then reinforced with cement-treated gravel over its entire thickness. The Young's modulus, E_s, for soil layer above the pipe was therefore greater than that for the bottom layer. The characteristics of the bonna concrete pipeline (48 m length), made up of 8 individual sections (each 6 m length), are: Young's modulus of concrete, $E_c = 36$ GPa (short-term strength), Poisson's ratio of concrete,

$\nu_c = 0.2$, Young's modulus of steel joint, $E_j = 210$ GPa, and Poisson's ratio of steel joint, $\nu_j = 0.3$. The characteristics of the surrounding ground are for the soil layer above the pipe: Young's modulus, $E_{s1} = 65$ MPa, friction angle, $\varphi'_{s1} = 25°$, Poisson's ratio, $\upsilon_{s1} = 0.3$, cohesion, $c_{s1} = 1$ kPa, and dry unit weight, $\gamma_{s1} = 20$ kN/m^3. For the soil layer below the pipe: Young's modulus, $E_{s2} = 15$ MPa, friction angle, $\varphi'_{s2} = 25°$, Poisson's ratio, $\upsilon_{s2} = 0.35$, cohesion, $c_{s2} = 1$ kPa, and dry unit weight, $\gamma_{s2} = 20$ kN/m^3.

The finite element mesh of the soil-pipe system is shown in Figure 6. Soil was modelled with two-dimensional finite triangular elements while the pipe was modelled with quadrilateral elements. Pipe was assumed to act in an isotropic and linearly elastic manner because the purpose of this model is to verify the ground strain measurements obtained on the site and not to assess the overall structural integrity of the pipe. A combination of self-weight (pipe, soil, water), pipe operating pressure and a static load of a truck can be easily introduced as loading inputs into the model. The depth of the natural ground corresponded to the dimension used in the literature, i.e., greater than 5 times the outsider diameter of the pipe (Rubio et al. 2007). The Mohr-Coulomb model to describe the soil behavior was used in the mechanical model. The interfaces between the soil and the structure and between two individual pipe segments were modelled using joint elements. These interfaces are considered as zero thickness interface elements in this study (Yáñez-Godoy et al. 2017b). A brief description of the basic theory for this type of element is given in (Potts et al. 2002). The interface stress is composed of both the normal and shear components for the joint element. This element is characterized by the compression elastic modulus and the shear elastic modulus. The Young's modulus of the soil, for both the upper and lower soil layers of the pipe, and the Young's modulus of steel joint were considered for the calculation of the joint element in the CAST3M software. No horizontal loading was considered in the pipe, which suggests that the pipe-soil system behaves as a rigid element without any influence from the numerical interfaces (i.e., it was assumed that there was not influence from joint elements in the 2-D model).

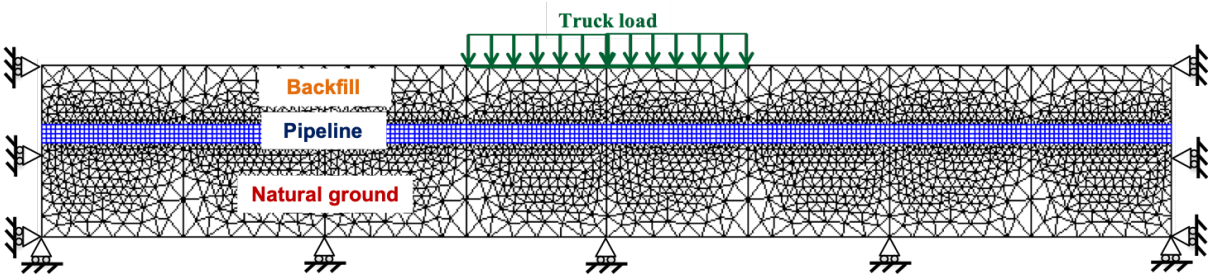

Fig. 6. *Finite element mesh of the soil–pipe system.*

IDENTIFICATION OF SOIL SPATIAL VARIABILITY FROM MEASUREMENTS

Methodology

This section introduces the methodology employed to identify the horizontal correlation length of the soil, according to the correlation model used, from the empirical semivariogram (Fig. 5b) and then to compute the scale of fluctuation. Two different methods can be used to identify this parameter: direct and inverse methods. The first method was briefly explored in

(Yanez-Godoy et al. 2018; Yáñez-Godoy et al. 2019) whereas the second method is commonly employed in the inverse problem (Soize 2017), if data are available, using the least squares or maximum likelihood method. The direct and inverse methods employ a common approach to create models of soil spatial variability: the spatial variability approach (Yáñez-Godoy et al. 2017b). This approach can be utilized in both of these methods owing to its ease of implementation. A Monte Carlo numerical simulation can thereafter be performed in each method to compute a mean semivariogram that fits a given empirical semivariogram.

The inverse method was utilized in this research. The available measures provide some information about parameters that could enable the characterization of the spatial variability observed at the site. Given the different ground strain measurement series above and below the pipeline (Fig. 3 and Fig. 4), which depend on the position of the optical fiber cable in the geotextile, it is interesting to identify the intervals of expected values of the parameters for characterizing the soil spatial variability along the pipeline. This method is commonly used for inverse problems (Soize 2017). The least-squares method (Molugaram et al. 2017) was employed to compute the main parameters of a semivariogram representing the soil spatial variability, according to the position of the geotextile (above or below the pipeline) and depending on the position of the optical fiber cable in the geotextile. The flowchart in Figure 7 illustrates the methodological approach used to identify the parameters characterizing the horizontal spatial structure of soil from an empirical semivariogram. The steps of this methodology are as follows:

Step 1, empirical semivariogram input: Different series are available according to the position of the optical fiber cable in the geotextile and the position of the geotextile, above or below the pipeline; for each series, an empirical semivariogram is obtained in this step and used as input data for the optimization problem in step 2.

Step 2, optimization problem solution: In this step, the minimization of an objective function that implies both the empirical semivariogram (step 1) and a computed semivariogram enable the determination of the adjustment of both horizontal correlation length and its corresponding sill value. The adjustment parameters are then used in step 3 to fit the computed mean semivariogram for each series.

Step 3, best fit of the mean computed semivariogram: The parameters obtained in step 2 are used to compute N simulations of a semivariogram, and a mean semivariogram is fitted for each series.

Step 4, identification of parameters characterizing the spatial structure of soil: In order to consider all different correlation models and series in step 3, the parameters characterizing the spatial structure of soil (mean and standard deviation of ground strain measurements and horizontal correlation length) are randomized for the case in which the geotextile is placed above or below the pipeline. As the horizontal correlation length parameter is related to the scale of fluctuation using the appropriate relationship for the chosen model (Table 1), the calculation of this parameter by using the different measurement series provides the methodology for characterizing the spatial structure of soil with a certain robustness.

Step 5, modelling of the measured ground strain: A numerical model of the instrumented pipeline is developed using CAST3M to calculate the ground strains along the pipeline in order to compare them with the measurements taken during an experimental test on the site.

Young's modulus of soil (commonly referred to as soil modulus) is a measure of soil stiffness and strain levels can be associated with this soil property. It was assumed that soil modulus characterizes the spatial randomness of the ground because soil modulus, which is a geomechanical property, is indirectly dependent on soil density and soil moisture, which are physical properties. In this way, a one-dimensional random field for this parameter was generated as the model input value using the correlation length identified in step 4.

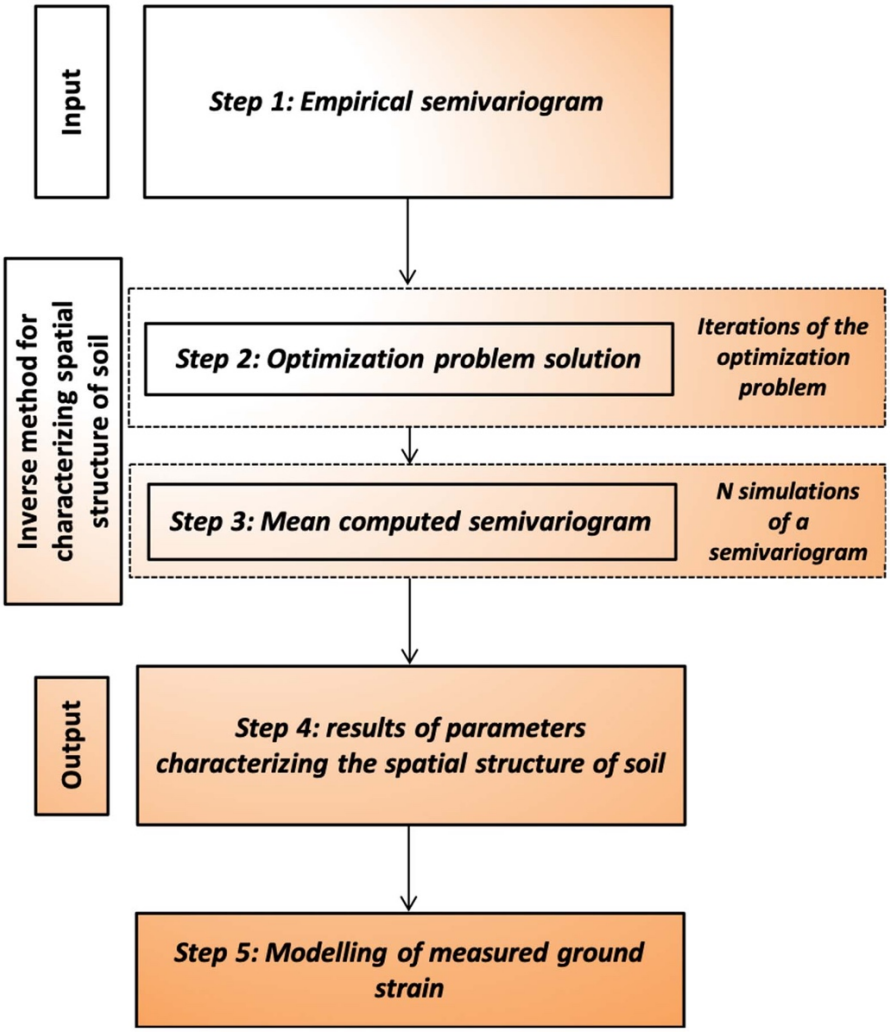

Fig. 7. *Flowchart of the methodology.*

Step 1: empirical semivariogram input

The ground strain measurement profiles presented in Figure 3 and Figure 4 are considered as spatial series. These spatial series were analyzed in this step by computing the empirical semivariogram. As highlighted before, ground strain measurement profiles above and below the pipeline for June 2017 were retained to analyze the spatial structure of the soil in more detail.

Empirical semivariogram above the pipeline

Figure 8a and Figure 8b present the empirical semivariograms above the pipeline computed for the measurements made in June 2017 for the ARSY, ALSY, and ALSO series. Figure 8a

shows that the empirical semivariogram for the roadside series, ARSY, has a lower semivariance value than those for the sidewalk series, ALSY and ALSO, as illustrated in Figure 8b. It can also be observed in these figures that for all series, the sill value is not constant. The sill value variations are larger for the sidewalk series. Indeed, these series present more scattered values than the roadside series, as indicated in the ground strain profile presented in Figure 3.

Empirical semivariogram below the pipeline

The empirical semivariograms below the pipeline for the measurements made in June 2017 were computed, as shown in Figure 8c and Figure d, for the BRSY, BRSO, BLSY, and BLSO series. These figures demonstrate that the sill values are different for each series. Indeed, two sills are clearly observed for the roadside series, particularly for BRSY (Fig. 8c), and for the sidewalk series, BLSY and BLSO (Fig. 8d). Regarding the roadside series, the sill values of the BRSY and BRSO series are very close in the first range between 3 and 5 m. The difference between sill values can be described by the most important local values observed in the ground strain measurement profile for the BRSY series shown in Figure 4. For the sidewalk series, Figure 4 indicates how the most important local values in the ground strain measurements for both the BLSY and BLSO series enable explanation of the variations of their sill values in the two ranges of the semivariogram.

Outcome of empirical semivariogram

The small sample of measures is not intended to ensure a direct statistical representation of δ_{emp}, but rather the empirical values observed in the different series in Figure 8 could provide an initial overview of the soil variability at the site. On the other hand, this sample of measures will enable the identification of a probabilistic distribution of the spatial variability of δ_{emp} by the inverse method. The observations obtained from the empirical semivariograms for δ_{emp} can be summarized as follows:

- For the series *above* the pipeline, δ_{emp} ranges from 5.8 m to 24.4 m, i.e., there is a ratio of approximately 4 between the upper and lower values. The mean value is approximately 13 m.
- For the series *below* the pipeline, δ_{emp} ranges from 2.4 m to 29.6 m, i.e., there is a ratio of approximately 12 between the upper and lower values. The mean value is approximately 12 m.

These observations reveal a wide variability range for the series below the pipeline, whereas the mean value is close for both series, above and below the pipeline.

Step 2: optimization problem solution

For each series above or below the pipeline (Fig. 8), the range or horizontal correlation length, δ_h, and sill, υ_h, are computed by solving an inverse problem. These parameters were determined according to the correlation model presented in Table 1. The optimization problem, $\lambda(\delta_h, \upsilon_h)$, is given by the least-squares method as follows (Eq. 5):

$$\lambda(\delta_h, \upsilon_h) = ArgMin[f, \{\delta_h, \upsilon_h\}] \quad (5)$$

with the objective function given by (Eq. 6):

$$f(\delta_h, \upsilon_h) = \sum(\bar{\gamma}(h)^c - \gamma(h)^e)^2 \quad (6)$$

where $\gamma(h)^e$ is the empirical semivariogram of spatial series (Eq. 4) and $\bar{\gamma}(h)^c$ is the computed semivariogram for the spatial series, which is the mean semivariogram result of 1000 simulations of the random field, $\varepsilon_x(x)$ (Eq. 3). The sum of each component of the objective function $(\bar{\gamma}(h)^c - \gamma(h)^e)^2$ is minimized after a number of iterations of the optimization problem (Eq. 5) using the Nelder-Mead simplex direct search algorithm (Lagarias et al. 1998). The termination criterion in this study was approximately 10^{-4}. Table 2 and Table 3 summarize the final values of the parameters computed by the inverse method for each series and considering different autocorrelation function models. The convergence of the computed parameters appears to be correct for 1000 simulations (a higher number of simulations than 1000 showed similar values).

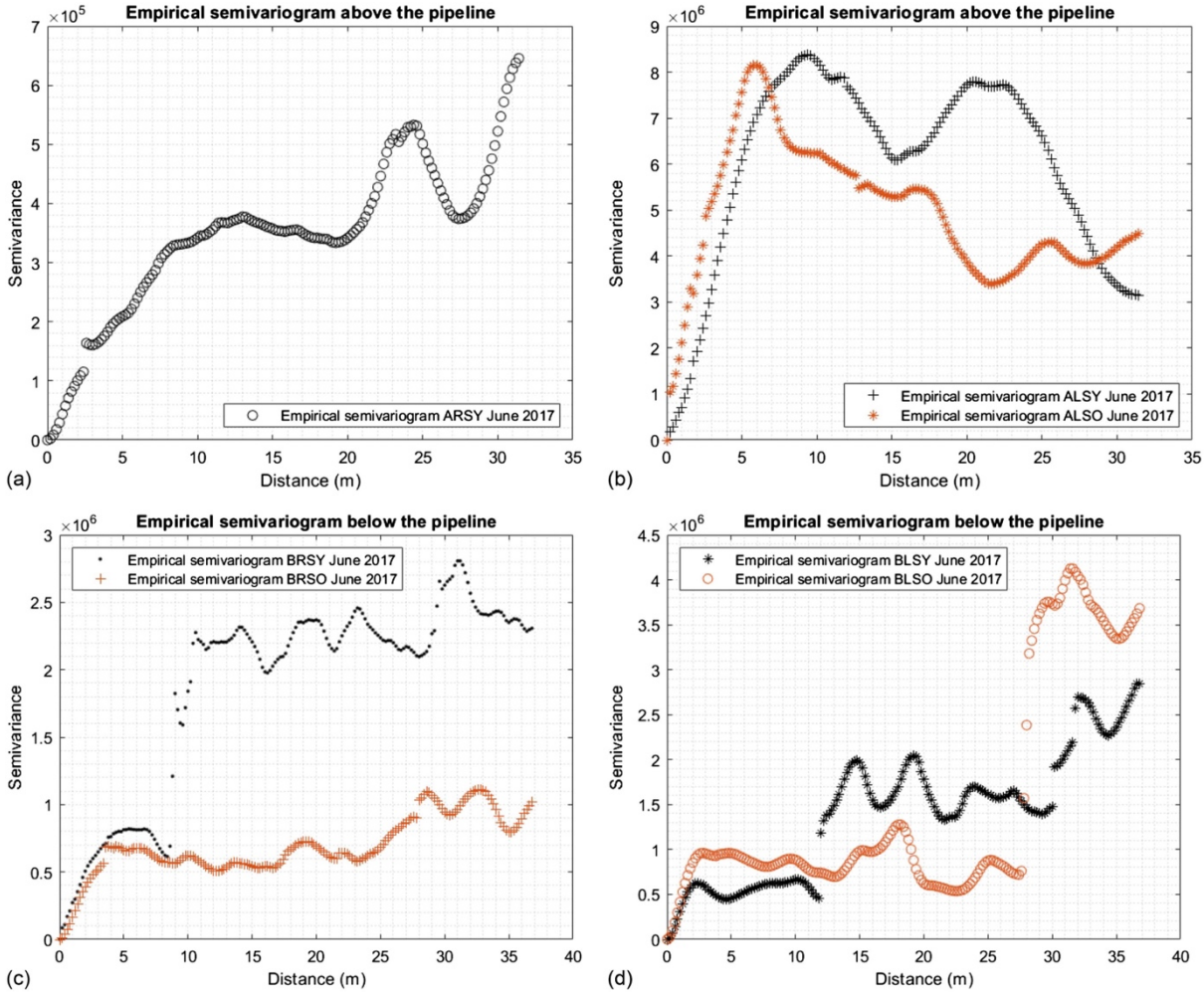

Fig. 8. *Empirical semivariograms of ground strain measurements above and below the pipeline made in June 2017: (a) ARSY series; (b) ALSY and ALSO series; (c) BRSY and BRSO series; and (d) BLSY and BLSO series.*

Step 3: best fit of the mean computed semivariogram

In this step, the mean computed semivariogram is obtained by averaging the semivariograms from random fields, $\varepsilon_x(x)$ (Eq. 3), generated by Monte Carlo simulations using the FFT method. As δ_h and v_h were computed in step 2, the number of simulations of random fields in this step can be increased (1x10^4 simulations) to obtain a smoother mean computed semivariogram for each series in Table 2 and Table 3. The computed semivariogram is then fitted to the empirical semivariogram by considering the different models of the autocorrelation function. As an example, Figure 9 presents the mean computed semivariogram for the BRSY series. Note that the mean computed semivariograms from the single exponential and cosine exponential models overlap; that is, the results are nearly identical for these models. Indeed, the computed values of δ_h and v_h are the same for both models and for each series, as shown in Table 2 and Table 3. The mean computed semivariograms for all series and autocorrelation function models agree well with the empirical semivariogram, except for the BLSO series. This last series does not seem to attain a sill in the range distance between 0 and 37 m. Indeed, the computed values of δ_h are significantly greater than the computed values in the other series. The BLSO series was not retained in the analysis in step 4.

Table 2. *Computed parameters by the inverse method, $\Delta_{case\ above\ pipeline}$*

Series	μ_h $[10^{-6}\ \mathrm{m/m}]$	Model	δ_h [m]	v_h	σ_h
ARSY	725.83	SE	8.02	0.45×10^6	670.82
		BN	10.49	0.41×10^6	640.31
		CE	8.02	0.45×10^6	670.82
		SOM	3.05	0.42×10^6	648.07
		SqE	6.15	0.41×10^6	640.31
ALSY	−247.51	SE	2.55	6.54×10^6	2557.34
		BN	5.57	6.54×10^6	2557.34
		CE	2.55	6.54×10^6	2557.34
		SOM	1.39	6.55×10^6	2559.30
		SqE	3.28	6.54×10^6	2557.34
ALSO	−229.19	SE	1.09	5.11×10^6	2260.53
		BN	2.66	5.11×10^6	2260.53
		CE	1.09	5.10×10^6	2258.32
		SOM	0.62	5.11×10^6	2260.53
		SqE	1.51	5.11×10^6	2260.53

Table 3. *Computed parameters by the inverse method,* $\Delta_{case\ below\ pipeline}$

Series	μ_h $[10^{-6}\ \mathrm{m/m}]$	Model	δ_h $[\mathrm{m}]$	v_h	σ_h
BRSY	654.43	SE	9.41	2.47×10^6	1571.62
		BN	13.51	2.30×10^6	1516.58
		CE	9.41	2.47×10^6	1571.62
		SOM	4.04	2.36×10^6	1536.23
		SqE	8.56	2.32×10^6	1523.15
BRSO	537.31	SE	4.64	0.78×10^6	883.18
		BN	4.16	0.73×10^6	854.40
		CE	4.64	0.78×10^6	883.18
		SOM	1.26	0.74×10^6	860.23
		SqE	2.53	0.73×10^6	854.40
BLSY	544.78	SE	24.7	2.72×10^6	1649.24
		BN	36.4	2.46×10^6	1568.44
		CE	24.7	2.72×10^6	1649.24
		SOM	6.93	2.10×10^6	1449.14
		SqE	12.79	1.92×10^6	1385.64

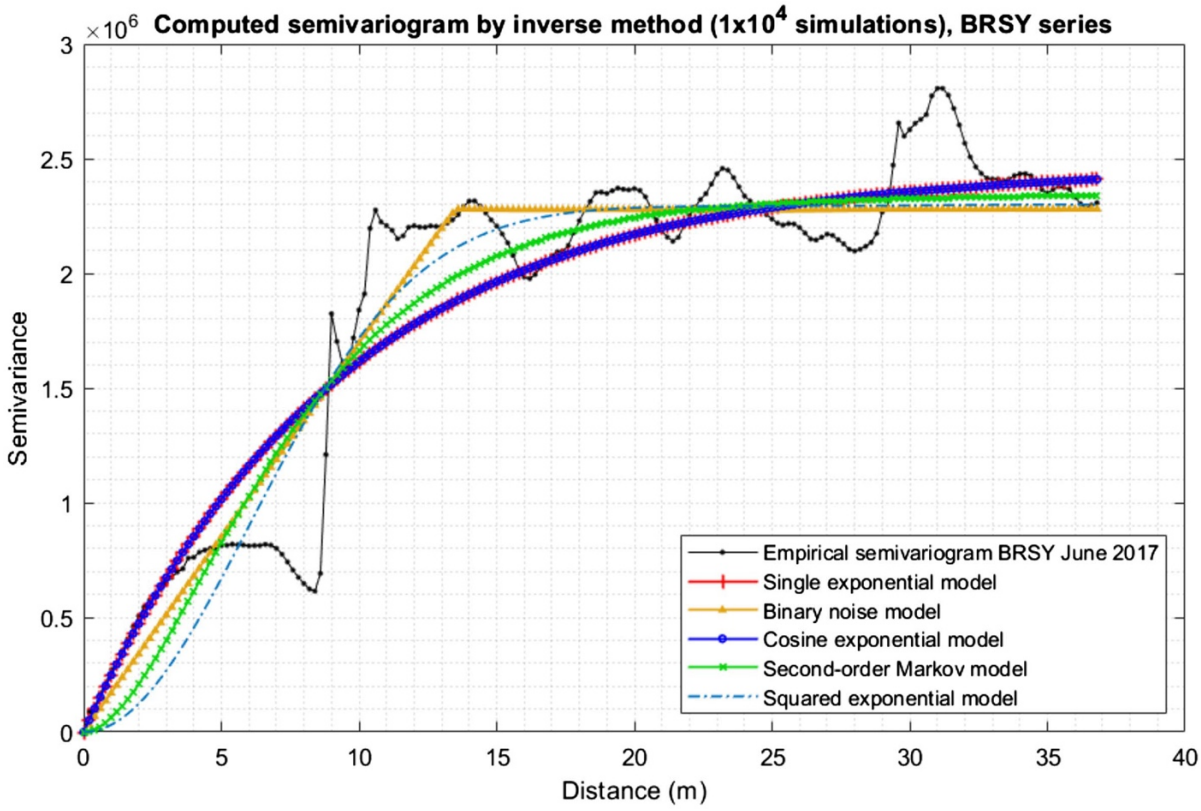

Fig. 9. *Mean semivariogram below the pipeline computed for the BRSY series.*

Step 4: results of the parameters characterizing the spatial structure of the soil

As can be observed in Table 2 and Table 3, δ_h depends on each series and differs according to the autocorrelation function model. A random variable for δ_h can then be considered to integrate the variability observed across the trench width (which corresponds to the position of each optical fiber cable embedded in the geotextile positioned above or below the pipeline) as well as the results obtained from the different models of the autocorrelation function. The mean of the measurements, μ_h, is not considered as a random variable because of the small number of values. The standard deviation of the measurements, σ_h, for each series was also considered as a random variable.

Step 4.1: establishment of parameter vectors

In this substep, μ_h, σ_h, and δ_h are gathered in vectors according to the individual case, above or below the pipeline, as follows (Table 2 and Table 3**)**:

- First, for each individual case (above or below the pipeline), a vector Δ_{case} is established using the different computed values of δ_h and $\sigma_h = \sqrt{v_h}$ and by adding μ_h, which corresponds to the mean value of measurements for each series.
- Second, an empirical distribution function of δ_h was built for each Δ_{case} (Fig. 10a and Fig. 10b). A histogram is considered for σ_h, which gives a uniform distribution in a certain interval for each Δ_{case} as shown in Figure 10c. The empirical distribution function of μ_h is not considered because of the small number of values. The calculated mean value for each Δ_{case} was as follows: $\mu_{h\ case\ above\ pipeline} = 83.04\ [10^{-6}\ \mathrm{m/m}]$ and $\mu_{h\ case\ below\ pipeline} = 578.84\ [10^{-6}\ \mathrm{m/m}]$.

Step 4.2: randomization of parameters

Different continuous probability distribution models (Shynk 2012) were tested to fit the empirical cumulative distribution function of δ_h for each Δ_{case} presented in Table 2 and Table 3. Maximum likelihood estimation (Shynk 2012) was used to find the best fit. As the correlation length is positive, the retained continuous probability distribution tested for this parameter has a positive domain. The three best fits of δ_h for each Δ_{case} are the Wald distribution (inverse Gaussian distribution), Birnbaum–Saunders distribution, and log-normal distribution. Figures 10a and Figure 10b illustrate these best fits for individual cases above and below the pipeline, $\Delta_{case\ above\ pipeline}$ and $\Delta_{case\ below\ pipeline}$, respectively.

As shown in Figure 10c, σ_h follows a uniform distribution for each Δ_{case}. A random uniform distribution is then considered as follows:

- For an individual case above the pipeline, $\Delta_{case\ above\ pipeline}$: $\mathcal{U}_{\sigma_h}(a, b)$, for $a = 500$ and $b = 3000$.
- For an individual case below the pipeline, $\Delta_{case\ below\ pipeline}$: $\mathcal{U}_{\sigma_h}(a, b)$, for $a = 800$ and $b = 1800$.

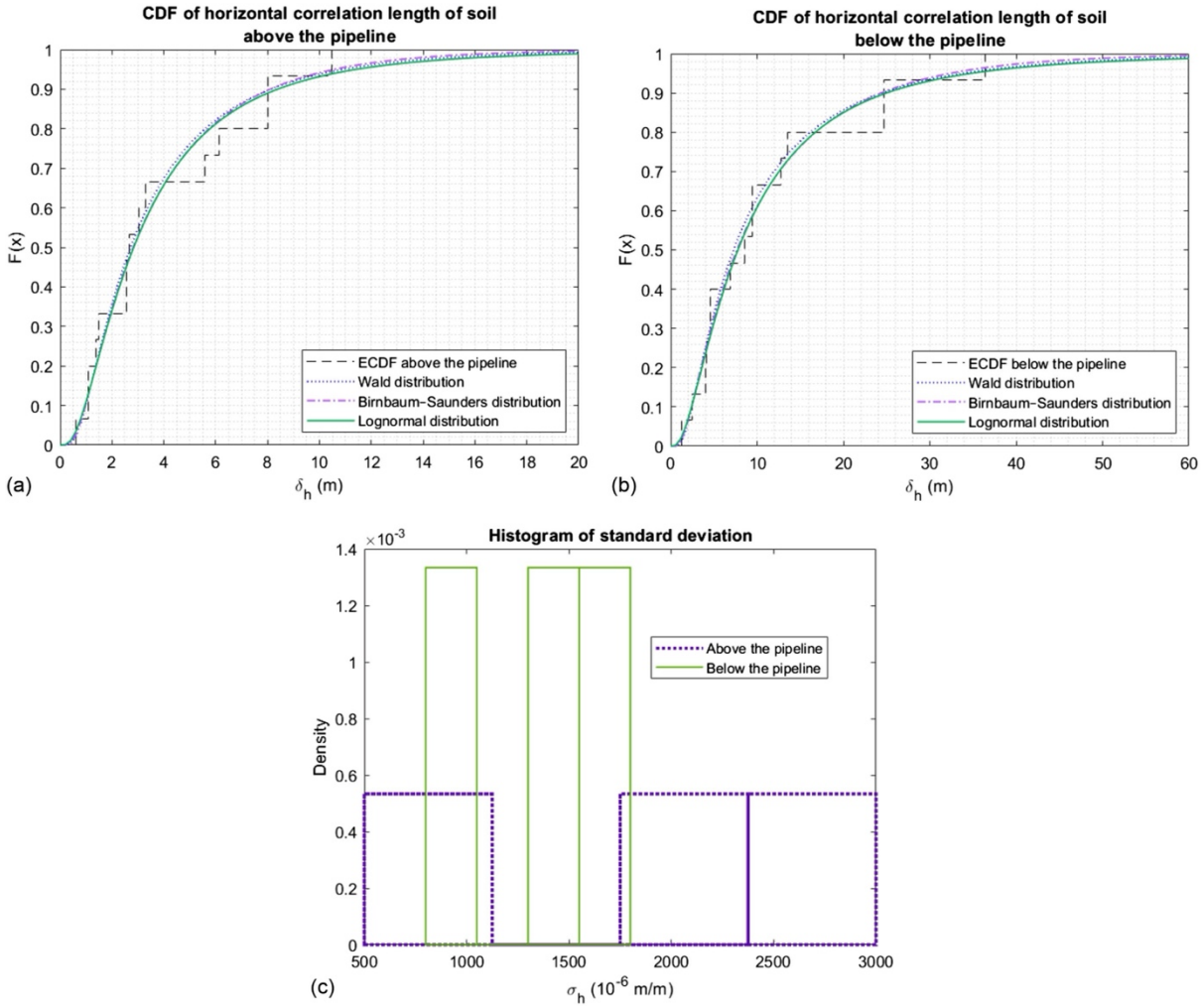

Fig. 10. *Variability of parameters characterizing the spatial structure of the soil: (a) correlation length above the pipeline; (b) correlation length below the pipeline; and (c) standard deviation above and below the pipeline.*

Step 5: modelling of the measured ground strain

A static load test of a truck parked at three different positions on the main axis of the pipe was carried out at the site: two positions near the ends of the pipe and one position near half the length of the pipe (in the range of distance between 40 and 55 m in Fig. 11). The results of the measurements taken in the central position were the most convincing to illustrate the modeling approach in this step. Two measurement situations at two different loading times were considered: a situation without the static load which constituted the time t_0 or reference time and another with the static load which constituted the time t_1. Measurements of ground strain above and below the pipeline with the static load of the truck were obtained, the latter are presented in Figure 11 and show very low values, in a range between $\pm$200 µm/m.

To simplify the uncertainty study in the 2-D numerical mechanical model (Fig. 6), the natural spatial randomness of the soil was considered by considering the soil modulus as a sensitive parameter. Soil modulus data was not available on the site. It was assumed, based on the only data available on the composition of the trench materials, a dense sandy soil for the soil layer above the pipe and a loose sandy soil for the layer below the pipe. A one-dimensional random field was considered to simulate the spatial variability of the soil. The other parameters

(geotechnical and geometrical parameters of the concrete pipe, external and internal loading) were considered as deterministic. A combination of self-weight (pipe, soil, water), pipe operating pressure (1200 kPa) and a static load of a truck (approximately 11 kPa applied to the backfill layer above the two center segments of the pipeline) was considered as input loading parameters.

The beta distribution was adopted to generate simulations of the soil modulus random field, above and below the pipeline in the horizontal direction of the soil, using the spatial variability approach. The limits of the beta distribution of the soil modulus were determined from the literature values (Bowles 2001; Buco 2007). For the soil layer above the pipe, the values considered were: minimum value, $E_{s1_{min}} = 50$ MPa, mean value, $E_{s1_{mean}} = 65$ MPa and maximum value, $E_{s1_{max}} = 80$ MPa. For the soil layer below the pipe, the values considered were: minimum value, $E_{s2_{min}} = 5$ MPa, mean value, $E_{s2_{mean}} = 15$ MPa and maximum value, $E_{s2_{max}} = 25$ MPa. A coefficient of variation, COV = 40%, was applied to the two mean values, $E_{s12_{mean}}$ and $E_{s2_{mean}}$; the standard deviation for each soil layer was then $\sigma_{E_s} = COV \times E_{s_{mean}}$. The beta probability distribution for each soil modulus is written, as follows (Yáñez-Godoy et al. 2017b) (Eq. 7):

$$E_s = \left(E_{s_{max}} - E_{s_{min}}\right) \times B + E_{s_{min}} \qquad (7)$$

where *B* is a beta random variable with values in $[0,1]$.The transition from a normal random field to a beta random field, $E_s(x)$, passes through the beta inverse cumulative distribution function, F^{-1}, which is obtained as follows (Eq. 8):

$$E_s(x) = F^{-1}(F(M(x)|\mu,\sigma)|a,b) \qquad (8)$$

where a, b are the parameters of the beta random variable *B* in (Eq. 7), $F(M(x)|\mu,\sigma)$ is the cumulative distribution function of a zero-mean, μ, normal random process, $M(x)$, with $\sigma = \sigma_{E_s}$. The random field is generated using the fast Fourier transform method. The generated $M(x)$ process was considered to associate a single exponential correlation function $\rho(\tau_h)$, where $\tau_h = 0.2$ m is the distance between data points in the random field. The correlation length in the horizontal direction of the soil, δ_h, for the soil modulus in each soil layer was considered for three different configurations as follows:

- First configuration: the spatial variability was not considered, which means that the modelling was carried out with the mean value of the soil modulus for each soil layer, above and below the pipeline.
- Second configuration: the spatial variability was only considered for the soil layer below the pipeline, the three values for δ_h were 1.8 m, 7.5 m and 34 m which corresponded to quantile values respectively of 5%, 50% and 95% from Figure 10b.
- Third configuration: the spatial variability was taken into account for both soil layers above and below the pipeline; for the upper soil layer, the three values for δ_h were 0.7 m, 2.8 m and 10.9 m which corresponded to quantile values respectively of 5%, 50% and 95% from Figure 10a; for the lower soil layer a single value for δ_h was considered, δ_h = 34 m, which corresponded to 95% quantile value from Figure 10b.

The configurations mentioned above (sources of uncertainty) as well as the 2-D numerical mechanical model (developed within CAST3M) are the first two steps in the uncertainty study performed here to compute the ground strain profile (defined as the quantity of interest in

the analysis ε_x). It is then necessary to move to the uncertainty propagation step through the 2-D model to transform the input uncertainty into a measure of uncertainty of the output. That is, to characterize the probabilistic content of ε_x. In a probabilistic framework, this requires estimating the probability density function of ε_x (Eq. 9):

$$\varepsilon_x = \mathcal{M}(x, d) \tag{9}$$

where $\mathcal{M}(.)$ is the 2-D model, x are the uncertain input parameters of the model and d are the deterministic inputs. The purpose is to obtain confidence intervals around the ground strain average profile in order to quantify the robustness of the predictions. The propagation of uncertainty was carried out by the direct Monte Carlo numerical simulation method. The authors have described the method in (Yáñez-Godoy et al. 2017b). The propagation of uncertainty is also extensively described in (Rocquigny et al. 2008). The spatial variability of the soil was modelled by generating 1000 simulations of a beta random field of the soil modulus for the two soil layers. Random fields were then entered into the finite element model to calculate ground strain profiles above and below the pipeline at the interfaces between the pipe and the soil layer, in the horizontal direction of the soil. The results of the model are shown in Figure 11 for the ground strain profiles below the pipeline for the first two configurations: the first configuration, without spatial variability, showed a ground strain profile of zero value with a slight variation in the loaded area between 40 and 55 m; the 95% confidence bounds for the second configuration showed that the smaller the value of δ_h, the wider the confidence bound of the ground strain profile. Most of the measurements, with the exception of those in the loaded area, are within the confidence bound where δ_h = 34 m. This shows that for a more loaded zone, a smaller value of δ_h is more meaningful to model the spatial variability of the soil. The results for the third configuration were very similar to those of the second configuration, when δ_h = 34 m, which means that the effect of the spatial variability of the upper layer has almost no impact on the calculated values of the lower layer.

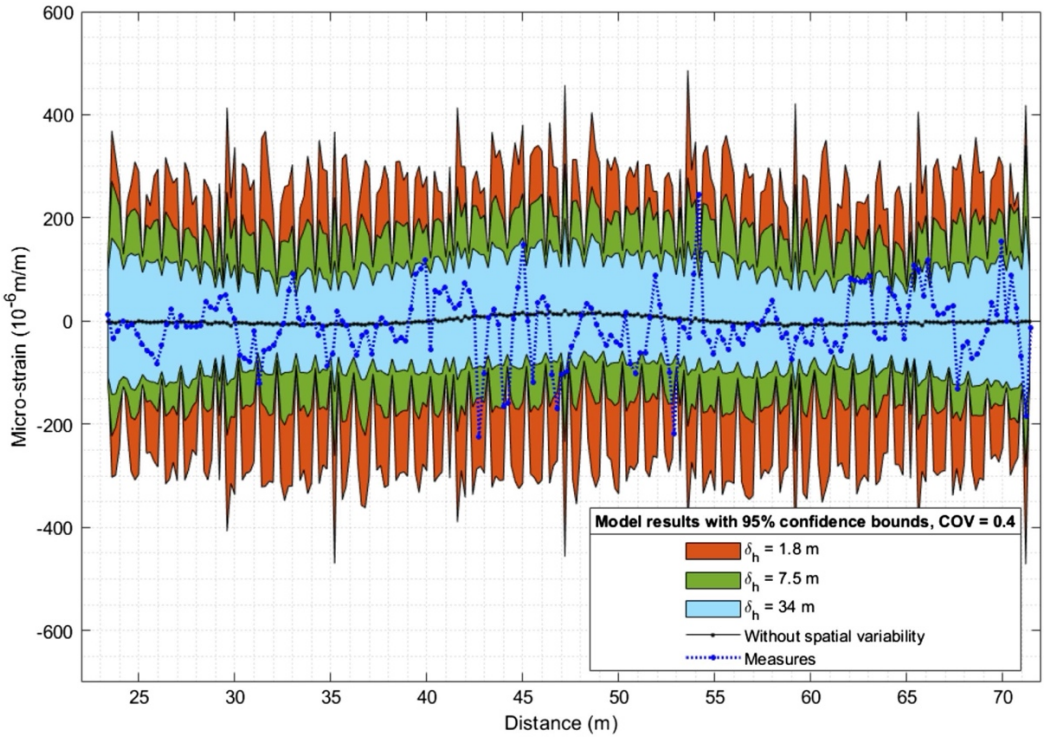

Fig. 11. *Measured and computed ground strains below the pipeline.*

DISCUSSION

It was assumed that differential settlement along the pipeline could result in spatial variability of the soil. The strain variation between June 2017 and August 2017 was very low (Fig. 3 and Fig. 4), which allow us to assume the stability of these differential settlements. The instrumentation settings implemented in the study area enabled ground strain measurements at different locations along both the length and width of the pipeline trench. The inverse method has the advantage of simultaneously considering the lengthwise and transverse spatial variability of the surrounding ground, above and below the pipeline. The use of different correlation functions to build random fields was also considered in this approach. These assumptions lead to the identification of an empirical cumulative distribution function of the mean horizontal correlation length of the soil as well as the best fits of the theoretical cumulative distribution functions. Another parameter that characterizes the spatial structure of soil is σ_h, which follows a uniform distribution for each Δ_{case}.

The statistical parameters of the empirical cumulative distribution function of δ_{h} (Table 2, Fig. 10a and Fig. 10b) showed a higher mean value for $\Delta_{case\ below\ pipeline}$ ($\mathrm{mean} = 11.2$ m) than for $\Delta_{case\ above\ pipeline}$ ($\mathrm{mean} = 3.9$ m). The coefficient of variation (COV) considering all the measurement series and different autocorrelation function models for $\Delta_{case\ below\ pipeline}$ is slightly larger ($COV = 0.9$) than that for $\Delta_{case\ above\ pipeline}$ ($COV = 0.8$). The envelope of fits of the cumulative distribution function presented in Figure 10a and Figure 10b has a confidence interval of 90% for δ_{h} for each individual case, Δ_{case}, as follows:

- For $\Delta_{case\ above\ pipeline}$: $\delta_{\mathrm{h}} = [0.7\ \mathrm{m};\ 10.9\ \mathrm{m}]$ and the median value is 2.8 m.
- For $\Delta_{case\ below\ pipeline}$: $\delta_{\mathrm{h}} = [1.8\ \mathrm{m};\ 34\ \mathrm{m}]$ and the median value is 7.5 m.

As observed in these confidence intervals, the upper limit for $\Delta_{case\ below\ pipeline}$, 34 m, is greater than the upper limit for $\Delta_{case\ above\ pipeline}$, 10.9 m. Nonetheless, the lower limit for $\Delta_{case\ above\ pipeline}$, 0.7 m, is smaller than the lower limit for $\Delta_{case\ below\ pipeline}$, 1.8 m. Further, the median value for $\Delta_{case\ below\ pipeline}$, 7.5 m, is greater than that for $\Delta_{case\ above\ pipeline}$, 2.8 m. These findings suggest that soil properties tend to be more variable above the pipeline than below the pipeline. However, larger scattering of the δ_{h} values is observed below the pipeline.

The model results showed that the spatial variability of the soil could correspond to the soil modulus parameter. Indeed, the measurements of ground strain taken during a static load test of a truck are included in the confidence bounds for three different values of δ_{h}. The horizontal correlation length of soil is an important determinant in understanding the behavior of the soil–pipe system (Yáñez-Godoy et al. 2019). Indeed, (Elachachi et al. 2004) showed that a buried concrete pipeline, composed of 3-m-long pipes, can present a homogeneous bending stress for small horizontal correlation lengths, and its variability is not significant vis-à-vis the global safety of the pipeline. However, for moderate horizontal correlation lengths, of 3 m to 30 m, bending stress is more variable and significant vis-à-vis the global safety of the pipeline. For values larger than 100 m, the bending stress becomes less variable. As a reminder, the instrumented pipeline presented in this paper is composed

of approximately 6-m-long pipes. The results seem to suggest that the horizontal correlation length of the soil below the pipeline, whose median value is larger than that above the pipeline, could have a more important effect on the structural integrity of the pipe. The model results showed that the spatial variability of the upper layer was not significant. Only the spatial variability below the pipeline could be considered to analyze the structural integrity of the pipe.

The findings presented in (Elachachi et al. 2004) were also studied in (Yáñez-Godoy et al. 2017a), in terms of the effect of the soil spatial variability of the soil on the structural integrity of a pipeline at a given time by considering only spatial variability below the pipeline. The results in (Yáñez-Godoy et al. 2017a) showed that for δ_{h} values between 6 and 18 m, the increase in the probability of failure of the pipeline (i.e., the reliability index decreases) is greater than for smaller values. It was also showed that the more the soil modulus dispersion increases, the more the reliability index decreases.

The obtained results show clearly that the conventional design by modeling the pipe only through its cross-section with the strong assumption that the embankment and the pipe bedding are homogenous, is largely insufficient. When considering the longitudinal dimension, the soil–pipe interaction and the soil variability should be included in the design. Such an approach will certainly help stakeholders in their asset management and allows them to identify earlier and more reliably the potential “black spots” of their technical assets from a geomechanical point of view.

CONCLUSION

Parameters to model the spatial variability of soil at an instrumented site for a buried feeder were obtained using the inverse method. Information concerning this variability is essential to study the structural behavior of a buried pipe because it elucidates the complexity of the soil–pipe system interaction, where the soil is a principal component of the system. The different ground strain measurements obtained at the site by a sensor-enabled geotextile showed signs of apparent stabilization of differential settlements below and along the pipeline some months after the pipeline was laid in its trench. More measurements would have been desirable in the period considered in this study; however, the contingences around the site led to some important reparations due to cable cuts, which were required to guarantee measurement continuity. These measurement profiles provide reference information to define a methodological approach to identify the parameters characterizing the horizontal spatial structure of soil from an empirical semivariogram function. This tool can be used in conjunction with random field theory and Monte Carlo simulations to compute the parameters of the semivariogram by the least-squares method. These parameters, the correlation length and measurement variance, represent the spatial variability of the soil. According to the sensor-enabled geotextile position and optical fiber cables in the geotextile, as well as the autocorrelation function model, the correlation length and measurement variance were randomized. The results show that for the two studied cases, above and below the pipeline, there are two different intervals of the horizontal correlation length of soil, with the soil layer above the pipeline being more variable than the ground below the feeder. The

model results showed that the spatial variability of the soil could correspond to the soil modulus parameter. The scale of fluctuation and the soil modulus parameter, were identified as important factors for enabling spatial variability characterization along the length and width of the trench in which the pipeline is laid and represent important factors for understanding the behavior of the soil–pipe system. These parameters can be used for comparison purposes on other sites to study the characterization of the spatial variability of the soil, and should be used as input parameters in a database to analyze the structural integrity of similar pipelines.

Data Availability Statement

Some or all data, models, or code that support the findings of this study are available from the corresponding author upon reasonable request (some ground strain measurements).

Acknowledgments

The authors would like to thank Syndicat des eaux d'Ile de France (SEDIF) and Veolia Eau d'Ile de France for their involvement in this project. Created in 1923, SEDIF is a public utility that is responsible for supplying drinking water to subscriber towns and municipalities in the Greater Paris area. SEDIF is the leading public drinking water utility in France and is one of the largest in Europe. Producing 765000 m^3 of water every day, SEDIF delivered 254 billion liters to users in 2019 through a network of pipes stretching 8767 km.

REFERENCES

Afnor. 1995a. "NF EN 639 Prescriptions communes pour tuyaux pression en béton y compris joints et pièces spéciales." Afnor Ed. Accessed September 20, 2022. https://www.boutique.afnor.org/fr-fr/norme/nf-en-639/prescriptions-communes-pour-tuyaux-pression-en-beton-y-compris-joints-et-pi/fa025553/10803.

Afnor. 1995b. "NF EN 641 Tuyaux pression en béton armé à âme en tôle, joints et pièces spéciales compris." Afnor Ed. Accessed September 20, 2022. https://www.boutique.afnor.org/fr-fr/norme/nf-en-641/tuyaux-pression-en-beton-arme-a-ame-en-tole-joints-et-pieces-speciales-comp/fa025555/10801.

Afnor. 2019. "NF EN 1295-1 Calcul de résistance mécanique des canalisations enterrées sous diverses conditions de charge - Partie 1 : prescriptions générales." Afnor Ed. Accessed September 27, 2022. https://www.boutique.afnor.org/fr-fr/norme/nf-en-12951/calcul-de-resistance-mecanique-des-canalisations-enterrees-sous-diverses-co/fa189189/82755.

Afnor. 2020. "NF P98-331 Chaussées et dépendances - Tranchées : ouverture, remblayage, réfection." Afnor Ed. Accessed September 27, 2022. https://www.boutique.afnor.org/fr-fr/norme/nf-p98331/chaussees-et-dependances-tranchees-ouverture-remblayage-refection/fa193146/85652.

Aslkhalili, A., H. Shiri, and S. Zendehboudi. 2021. “Probabilistic Assessment of Lateral Pipeline–Backfill–Trench Interaction.” J. Pipeline Syst. Eng. Pract., 12 (3): 04021034. American Society of Civil Engineers. https://doi.org/10.1061/(ASCE)PS.1949-1204.0000564.

Becerril García, D., J. Cortés-Pérez, and I. D. Moore. 2020. “Modelling and parametric study of a gasketed bell and spigot joint in a buried high density polyethylene pipeline.” Tunn. Undergr. Space Technol., 98: 103325. https://doi.org/10.1016/j.tust.2020.103325.

Bouayad, D. 2017. “Assessment of Sandy Soil Variability Based on CPT Data.” Procedia Eng., Proceedings of the 1st International Conference on the Material Point Method (MPM 2017), 175: 310–315. https://doi.org/10.1016/j.proeng.2017.01.033.

Bowles, J. E. 2001. Foundation Analysis and Design. Norwich, NY: McGraw-Hill.

Breysse, D., C. La Borderie, S. M. Elachachi, and H. Niandou. 2007. “Spatial variations in soil properties and their influence on structural reliability.” Civ. Eng. Environ. Syst., 24 (2): 73–83. Taylor & Francis. https://doi.org/10.1080/10286600601156673.

Buco, J. 2007. “Analyse et modélisation du comportement mécanique des conduites enterrées.” These de doctorat. Lyon, INSA.

Chilès, J.-P., and P. Delfiner. 2012. Geostatistics: Modeling Spatial Uncertainty. Wiley.

Ching, J., T.-J. Wu, A. W. Stuedlein, and T. Bong. 2018. “Estimating horizontal scale of fluctuation with limited CPT soundings.” Geosci. Front., Reliability Analysis of Geotechnical Infrastructures, 9 (6): 1597–1608. https://doi.org/10.1016/j.gsf.2017.11.008.

Cressie, N. 2015. Statistics for Spatial Data, Revised Edition.

Darwich, G. 2019. “Modélisation du comportement géo-mécanique d’une conduite de transfert et évaluation de sa performance en contexte incertain. - TEL - Thèses en ligne.” Bordeaux, France: Université de Bordeaux.

Elachachi, S. M., D. Breysse, and A. Denis. 2012. “The effects of soil spatial variability on the reliability of rigid buried pipes.” Comput. Geotech., 43: 61–71. https://doi.org/10.1016/j.compgeo.2012.02.008.

Elachachi, S. M., D. Breysse, and L. Houy. 2004. “Longitudinal variability of soils and structural response of sewer networks.” Comput. Geotech., 31 (8): 625–641. https://doi.org/10.1016/j.compgeo.2004.10.003.

Froio, D., and E. Rizzi. 2017. “Analytical solution for the elastic bending of beams lying on a linearly variable Winkler support.” Int. J. Mech. Sci., 128–129: 680–694. https://doi.org/10.1016/j.ijmecsci.2017.04.021.

Galindez-Jamioy, C. A., and J. M. López-Higuera. 2012. “Brillouin Distributed Fiber Sensors: An Overview and Applications.” J. Sens., 2012: 17. Hindawi. https://doi.org/10.1155/2012/204121.

Grynyshyna-Poliuga, O. 2019. “Characteristic of modelling spatial processes using geostatistical analysis.” Adv. Space Res., 64 (2): 415–426. https://doi.org/10.1016/j.asr.2019.04.020.

Higgins, M. S., A. Stroebele, and S. Zahidi. 2012. “Numbers Don’t Lie: PCCP Performance and Deterioration Based on a Statistical Review of a Decade of Condition Assessment Data.” Proc. Pipelines 2012 Conf., 298–306. Miami Beach, Florida: Edited by Robert J. Card, P.E., M.ASCE; and Michael K. Kenny, M.ASCE.

Iten, M., Z. Spera, J. K. Jeyapalan, G. Duckworth, D. Inaudi, X. Bao, N. Noether, A. Klar, A. Marshall, B. Glisic, M. Facchini, J. Jason, M. Elshafie, C. Kechavarzi, W. Miles, S. Rajah, B. Johnston, J. Allen, H. Lee, S. Leffler, A. Zadok, P. Hayward, K. Waterman, and O. Artieres. 2015. “Benefits of Global Standards on the Use of Optical Fiber Sensing Systems for the Impact of Construction of New Utilities and Tunnels on Existing Utilities.” Pipelines 2015, 1655–1666. Baltimore, Maryland: American Society of Civil Engineers.

Jaksa, M., W. Kaggwa, and P. Brooker. 1999. “Experimental evaluation of the scale of fluctuation of a stiff clay.” Proc. 8th Int. Conf. Appl. Stat. Probab. Civ. Eng. ICASP8, 415–422.

Joshi, S., A. Prashant, A. Deb, and S. K. Jain. 2011. “Analysis of buried pipelines subjected to reverse fault motion.” Soil Dyn. Earthq. Eng., 31 (7): 930–940. https://doi.org/10.1016/j.soildyn.2011.02.003.

Kleiner, Y., and B. Rajani. 2001. “Comprehensive review of structural deterioration of water mains: statistical models.” Urban Water, Ground Water in the Environment, 3 (3): 131–150. https://doi.org/10.1016/S1462-0758(01)00033-4.

Lagarias, J. C., J. A. Reeds, M. H. Wright, and P. E. Wright. 1998. “Convergence Properties of the Nelder–Mead Simplex Method in Low Dimensions.” SIAM J Optim., 9 (1): 112–147. https://doi.org/10.1137/S1052623496303470.

Liu, Z., Y. Kleiner, B. Rajani, L. Wang, and W. Condit. 2012. Condition Assessment Technologies for Water Transmission and Distribution Systems. 134. National Risk Management Research Laboratory, EPA United States Environmental Protection Agency.

McGrath, T., R. Chambers, and P. Sharff. 1990. “Recent Trends in Installation Standards for Plastic Pipe.” STP1093-EB Buried Plast. Pipe Technol., 281–293. ASTM International. https://doi.org/10.1520/STP42126S.

Molugaram, K., G. S. Rao, A. Shah, and N. Davergave. 2017. Statistical Techniques for Transportation Engineering. Oxford, United Kingdom ; Cambridge, MA: Butterworth-Heinemann.

Nie, X., J. Zhang, H. Huang, Z. Liu, and S. Lacasse. 2015. “Scale of Fluctuation for Geotechnical Probabilistic Analysis.” 5th Int. Symp. Geotech. Saf. Risk. Rotterdam, The Netherlands.

Onyejekwe, S., X. Kang, and L. Ge. 2016. “Evaluation of the scale of fluctuation of geotechnical parameters by autocorrelation function and semivariogram function.” Eng. Geol., 214: 43–49. https://doi.org/10.1016/j.enggeo.2016.09.014.

Oswell, J. M., J. Hart, and N. Zulfiqar. 2019. “Effect of Geotechnical Parameter Variability on Soil-Pipeline Interaction.” J. Pipeline Syst. Eng. Pract., 10 (4): 04019028. American Society of Civil Engineers. https://doi.org/10.1061/(ASCE)PS.1949-1204.0000402.

Phoon, K.-K. (Ed.). 2014. Reliability-Based Design in Geotechnical Engineering: Computations and Applications. CRC Press.

Potts, D., Axelsson, K., Grande, L., Schweiger, H., and Long, M. 2002. Guidelines for the Use of Advanced Numerical Analysis. Thomas Telford.

Rajani, B., and Y. Kleiner. 2001. “Comprehensive review of structural deterioration of water mains: physically based models.” Urban Water, Ground Water in the Environment, 3 (3): 151–164. https://doi.org/10.1016/S1462-0758(01)00032-2.

Rajeev, P., and J. Kodikara. 2014. “Factors contributing to large diameter water pipe failure.” Water Asset Manag. Int., 10 (3): 9–14.

Rocquigny, E. de, N. Devictor, and S. Tarantola. 2008. Uncertainty in Industrial Practice: A Guide to Quantitative Uncertainty Management. Chichester, England ; Hoboken, NJ: Wiley–Blackwell.

Romer, A. E., G. E. C. Bell, and R. D. Ellison. 2007. “Failure of Prestressed Concrete Cylinder Pipe.” Proc. ASCE Int. Conf. Pipeline Eng. Constr., 1–17. Boston, Massachusetts, United States: Edited by Mohammad Najafi, P.E. Lynn Osborn, P.E.

Rubio, N., D. Roehl, and C. Romanel. 2007. “A THREE DIMENSIONAL CONTACT MODEL FOR SOIL-PIPE INTERACTION.” https://doi.org/10.2140/JOMMS.2007.2.1501.

Sahraoui, Y., M. Benamira, M. Nahal, F. Nouadria, and A. Chateauneuf. 2020. “The effect of welded joint repair on a corroded pipeline reliability subjected to the hardness spatial variability and soil aggressiveness.” Eng. Fail. Anal., 118: 104854. https://doi.org/10.1016/j.engfailanal.2020.104854.

Shynk, J. J. 2012. Probability, random variables, and random processes theory and signal processing applications. Wiley.

Soize, C. 2017. Uncertainty Quantification: An Accelerated Course with Advanced Applications in Computational Engineering. Springer.

Uzielli, M., S. Lacasse, F. Nadim, and K.-K. Phoon. 2006. “Soil Variability Analysis for Geotechnical Practice.” Proc. 2nd Int. Workshop Characterisation Eng. Prop. Nat. Soils. Singapore.

Vanmarcke, E. H. 1977. “Probabilistic Modeling of Soil Profiles.” J. Geotech. Eng. Div., 103 (11): 1227–1246. ASCE.

Wang, W., Y. Wang, B. Zhang, W. Shi, and C.-Q. Li. 2021. “Failure prediction of buried pipe network with multiple failure modes and spatial randomness of corrosion.” Int. J. Press. Vessels Pip., 191: 104367. https://doi.org/10.1016/j.ijpvp.2021.104367.

Xu, M., and D. Shen. 2020. “The influence of erosion voids on the longitudinal behaviour of a jointed large-diameter reinforced concrete pipeline.” Tunn. Undergr. Space Technol., 103: 103494. https://doi.org/10.1016/j.tust.2020.103494.

Yanez-Godoy, H., G. Darwich, S. M. Elachachi, O. Chesneau, and C. Feliers. 2018. “Suivi du comportement mécanique d’une conduite d’eau potable enterrée et instrumentée : analyse des premières mesures.” Acad. J. Civ. Eng., 36 (1): 629–632. https://doi.org/10.26168/ajce.36.1.136.

Yáñez-Godoy, H., S. M. Elachachi, and G. Darwich. 2017a. “Geomechanical behaviour of large diameter pressure water pipelines in unidimensional heterogeneous soils.” Saf. Reliab. Risk

Resil. Sustain. Struct. Infrastruct. Proc. 12th Int. Conf. Struct. Saf. Reliab., 386–395. Vienna, Austria: C. Bucher, B.R. Ellingwood, D.M. Frangopol (eds.).

Yáñez-Godoy, H., S.-M. Elachachi, O. Chesneau, and C. Feliers. 2019. “Identification of key determinants of geo-mechanical behavior of an instrumented buried pipe.” Proc. 13th Int. Conf. Appl. Stat. Probab. Civ. Eng. ICASP13, 1297–1304. Korean Institute of Bridge and Structural Engineers.

Yáñez-Godoy, H., A. Mokeddem, and S. M. Elachachi. 2017b. “Influence of spatial variability of soil friction angle on sheet pile walls’ structural behaviour.” Georisk Assess. Manag. Risk Eng. Syst. Geohazards, 11 (4): 299–314. https://doi.org/10.1080/17499518.2017.1297465.

Yang, J.-N. 1972. “Simulation of random envelope processes.” J. Sound Vib., 21 (1): 73–85. https://doi.org/10.1016/0022-460X(72)90207-6.

Zheng, Q., L. Graf-Alexiou, Y. Li, N. Yoosef-Ghodsi, M. Fowler, M. Kainat, and S. Adeeb. 2021. “Strain demand of elastic pipes subjected to permanent ground displacements using the finite difference method.” J. Pipeline Sci. Eng., Special Issue on Strain-Based Assessment and Design of Pipelines, 1 (2): 176–186. https://doi.org/10.1016/j.jpse.2021.06.001.